




Article

# Archaeometric Approach for Studying Architectural Earthenwares from the Archaeological Site of S. Omobono (Rome-Italy)

Domenico Miriello <sup>1,\*</sup>, Fabrizio Antonelli <sup>2</sup>, Andrea Bloise <sup>1</sup>, Monica Ceci <sup>3</sup>, Stefano Columbu <sup>4</sup>, Raffaella De Luca <sup>1,\*</sup>, Marco Lezzerini <sup>5</sup>, Alessandra Pecci <sup>6</sup>, Bina Sara Mollo <sup>1</sup> and Paolo Brocato <sup>7</sup>

<sup>1</sup> Department of Biology, Ecology and Earth Science (DiBEST), Università della Calabria, Via P. Bucci, 87036 Arcavacata di Rende (CS), Italy; andrea.bloise@unical.it (A.B.); saramollo@gmail.com (B.S.M.)

<sup>2</sup> Laboratory for the Analysis of Ancient Materials (LAMA), University Iuav of Venice, San Polo 2468, 30125 Venice (VE), Italy; fabrizio.antonelli@iuav.it

<sup>3</sup> Sovrintendenza Capitolina ai Beni Culturali, Roma Capitale, Piazza Lovatelli, 35, 00186 Roma (RM), Italy; monica.ceci@comune.roma.it

<sup>4</sup> Department of Chemical and Geological Sciences, University of Cagliari, Cittadella universitaria, 09042 Monserrato (CA), Italy; columbus@unica.it

<sup>5</sup> Department of Earth Sciences, University of Pisa, Via S. Maria 53, 56126 Pisa (PI), Italy; marco.lezzerini@unipi.it

<sup>6</sup> ERAAUB, Department of History and Archaeology, University of Barcelona, c/Montalegre 4, 6, 08001 Barcelona, Spain; alepecci@gmail.com

<sup>7</sup> Department of Humanistic Studies, University of Calabria, Via P. Bucci, 87036 Arcavacata di Rende (CS), Italy; paolo.brocato@tin.it

\* Correspondence: miriello@unical.it (D.M.); raffaella.deluca@unical.it (R.D.L.)

Received: 27 February 2019; Accepted: 29 April 2019; Published: 30 April 2019



**Abstract:** This paper reports the findings of an archaeometric study performed on 14 architectural earthenwares from the archaeological site of S. Omobono, located in the historic center of Rome (Italy). The archaeological site, accidentally discovered in 1937, includes the remains of a sacred area previously occupied by two temples, one of which was converted into the church of S. Omobono, in 1575. The samples, dated between the 7th and the 6th century BC, belong to different sectors of the site. Their petrographic, mineralogical and geochemical characterization was performed by optical microscopy (OM), X-ray powder diffraction (XRPD), X-ray fluorescence (XRF), electron probe micro-analysis (EPMA), and Raman spectroscopy (RS). The compositional data obtained were also subjected to the principal component analysis (PCA) in order to highlight similarities and differences among the samples. By combining geochemical and petrographic data, we were able to identify several different fabrics. Furthermore, the study provided valuable information on the firing temperatures of some samples and the provenance of the raw materials, by analyzing the chemical composition of clinopyroxenes present as non-plastic inclusions.

**Keywords:** archaeometry; fabric; firing temperature; clinopyroxene; provenance; constructive phases

## 1. Introduction

The archaeological site of S. Omobono is located between the Capitoline Hill and the Tiber River in the historic center of Rome (Italy). Over the centuries, the area has been subjected to several transformations. The site was originally occupied by the archaic temple, whose first construction phase dates back to the period of King Servius Tullius (570-560 BC) and its second phase to the period

between 540–530 BC ca. At the beginning of the 5th century BC the archaic temple was destroyed and replaced by a large podium on which twin temples, dedicated to the goddesses Fortuna and Mater Matuta. These two temples were then destroyed and rebuilt several times until the 6th century AD, when the Temple of Mater Matuta was converted into a Christian church. Over the centuries, the church underwent major restoration interventions and in 1575 it was dedicated to S. Omobono [1], from whom the archaeological site takes its name. This area was accidentally discovered in 1937 during the construction of a new building. Subsequently, a large number of studies was carried out on the site [2–4] and numerous excavations were performed, providing a valuable insight into the activities conducted in the area from the archaic period to the Republican and Imperial age and after that the pagan temple had been converted into a Christian church. Over the years, nine trenches (I, II, III, IV, V, VI, VII, now called D10, IX, X) were opened, while sector III has yet to be excavated [5,6].

Earthenwares and ceramic materials in general, are usually found in great abundance in most archaeological sites. As demonstrated by numerous scientific studies [7–17], these materials bear the potter’s mark and enhance our understanding of trade and everyday life in the area in which they were found. For this reason, their archaeometric study, together with the study of natural and artificial stone materials [18–34], is essential not only for identifying the raw materials and the production technology adopted, but also to obtain information about the history and the evolution of the monument or of the archaeological site analyzed.

In this study, 14 samples of architectural earthenwares, belonging to the archaic temple and collected from different sectors of the archaeological site (Table 1) were studied. The samples, which belong to the earliest period of ancient Rome and cover a period between the end of the 7th century and the 6th century BC, were analyzed using an archaeometric approach based on the application of various analytical techniques.

**Table 1.** Architectural earthenwares coming from the archaeological site of S. Omobono, with typology, layer, provenance area and historical period, based on archaeological data.

Sample	Typology	Layer and Inventory Number	Sector	Historical Period Based on Archaeological Data
S3	<i>Impasto rosso</i> pan-tile	Layer 877 (n. MA11081)	D 10	End of 7th–begin of 6th century BC
S4	<i>Impasto rosso</i> pan-tile	Layer 5 (n. 925)	VII-IX	End of 7th–begin of 6th century BC
S7	<i>Impasto rosso</i> pan-tile	Layer 1244 (n. 1102)	A7	End of 7th–begin of 6th century BC
S9	<i>Impasto chiaro sabbioso</i> pan-tile	Layer 883 (n. 1080)	D 10	6th century BC (probably 580–520)
S10	<i>Impasto chiaro sabbioso</i> pan-tile	Layer 1208 (n. MA1 1054)	D 10	6th century BC (probably 580–520)
S11	<i>Impasto chiaro sabbioso</i> pan-tile	Layer 1214 (n. MA3 1044)	D 10	6th century BC (probably second half)
S12	<i>Impasto chiaro sabbioso</i> pan-tile	Layer 23 (n. 956)	I	6th century BC (probably 580–520)
S13	<i>Impasto chiaro sabbioso</i> pan-tile	Layer 10 (n. 1026)	Gjerstad excavation	6th century BC (probably 580–520)
S15	<i>Impasto chiaro sabbioso</i> cover-tile	Layer 1207 (n. 1207)	D 10	6th century BC (probably 580–520)
S17	<i>Impasto chiaro sabbioso</i> cover-tile	Layer 1213 (n. 1067)	D 10	6th century BC (probably 580–520)
S18	<i>Impasto chiaro sabbioso</i> cover-tile	Layer 1221 (n. 1075)	D 10	6th century BC (probably 580–520)
S21	Fragment of pediment slab	Layer 7 (n. 966)	II	6th century BC (about 580)
S22	Architectural decoration (fragment of panther)	Layer 1214	D 10	6th century BC (about 580)
S23	Architectural decoration (fragment of voluta)	Layer 1214	D 10	6th century BC (about 540)

The study, carried out in this work, is not casual; in fact the archaeological site of S. Omobono has an important scientific relevance: It represents a fundamental piece relative to the origin of the city. Indeed, the site consists of a sacred area strictly connected to the Porto Tiberino which represented the connection between the city of Rome and the Mediterranean [35]. In addition, at the present state of research, the archaic temple represents the first religious building, in archaic Rome, made of stone [36].

The only study about earthenwares from the site of S. Omobono was performed by Ammerman et al. [37], who identified the presence of a main fabric in the site. However, a greater complexity than that highlighted by Ammerman et al. [37], has been revealed in this study, as reported by the following results.

The principal aim of our work is to determine the mineralogical, petrographic and chemical composition of the architectural earthenwares in order to identify the raw materials used and, consequently, to formulate hypothesis on their possible provenance and to obtain information about their production technology. Indeed, all the data obtained may represent a useful term of comparison for other studies dealing on other ceramic materials coming from the same archaeological site or from other contexts of ancient Rome.

## 2. Materials and Methods

The samples were collected in various sectors of the archaeological site of S. Omobono, including the archaic temple and the cell located in the West Temple (Figure 1 and Table 1). More specifically, eleven tile samples (samples S3–S18), one fragment of pediment slab (S21), and two samples of architectural elements and decorations (S22 and S23), dated between the 7th and the 6th century BC, were collected (Table 1).

All of the samples were studied in thin sections under polarized light microscopy (OM), using a Zeiss Axioskop 40 petrographic microscope (Zeiss, Jena, Germany), equipped with a Canon PowerShot A640 photo camera (Canon, Tokyo, Japan). The roundness and the sorting of the non-plastic inclusions were defined using qualitative visual estimation charts [38–40]; the semi-quantitative estimate of the percentages of non-plastic inclusions, matrix and macroporosity ( $d > 1/16$  mm) as volume fractions were obtained by comparing the thin sections observed under optical microscopy with visual charts [41,42].

The mineralogical analysis was performed by X-ray powder diffraction (XRPD), through a Bruker D8 Advance X-ray powder diffractometer (Bruker, Karlsruhe, Germany), with Cu-K $\alpha$  radiation, operating at 40 kV and 20 mA. The scans were collected with a step scan of  $0.02^\circ 2\theta$  and 2 s/step, in the range  $3\text{--}60^\circ 2\theta$ . The width of the divergence, anti-scattering and receiving slits were of 0.6, 0.2, and 0.1 mm, respectively [43]. To identify the mineralogical phases in each X-ray powder spectrum, DIFFRACplus EVA V. 11.3 software program (Bruker, Karlsruhe, Germany) was used, by comparing experimental peaks with PDF2 reference patterns. An estimate of the mineralogical phases present in the samples was obtained by Rietveld refinements [44,45] carried out using TOPAS software V.4.2 (Bruker, Karlsruhe, Germany).

The chemical composition of major, minor (SiO<sub>2</sub>, TiO<sub>2</sub>, Al<sub>2</sub>O<sub>3</sub>, Fe<sub>2</sub>O<sub>3</sub>, MnO, MgO, CaO, Na<sub>2</sub>O, K<sub>2</sub>O, and P<sub>2</sub>O<sub>5</sub>) and trace (Ni, Cr, V, La, Ce, Co, Nb, Ba, Y, Sr, Zr, Zn, Rb, and Pb) elements was determined by X-ray fluorescence (XRF), using a Bruker S8 Tiger WD X-ray fluorescence spectrometer (Bruker, Karlsruhe, Germany), with a rhodium tube (intensity 4 kW and XRF beam of 34 mm). The analysis was carried out on pressed powder pellets placed over boric acid, using 6 g of specimen (maximum working pressure 25 bar). The chemical data were processed by Aitchison's model [46–48], in order to calculate the centred log ratio transformations (CRL), and the coefficients obtained were processed with the principal component analysis (PCA).

Detailed analyses were also performed using Raman spectroscopy with a Thermo Fisher DXR Raman Microscope and OMNICxi Raman Imaging software 1.0 (Waltham, MA, USA). The 532.0-nm line was used at an incident power output variable ranging between 3 and 7mW. The spectra obtained were compared with the spectra available in the database of the Department of Biology, Ecology and Earth Sciences (DiBEST) at the University of Calabria and the RRUFF Project database.

An Electron Probe Micro Analysis (EPMA) was carried out on the clinopyroxenes with an Electron Probe Micro Analyser JEOL-JXA 8230 and a W/LaB6 source (Jeol, Tokyo, Japan) equipped with 5 Spectrometers WDS with LDE, TAP, PETJ and LiF crystals.

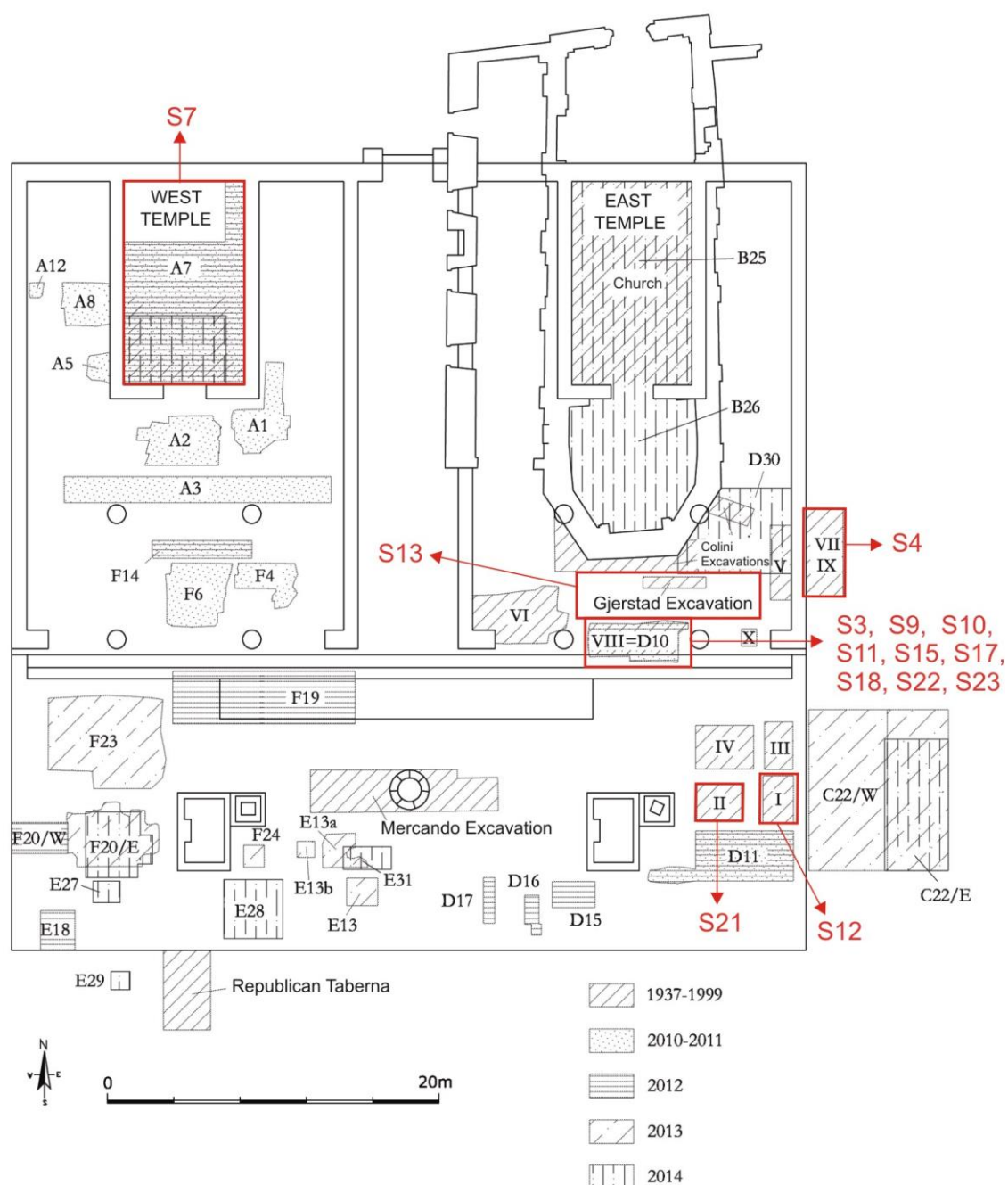


**Figure 1.** Map of the archaeological site of S. Omobono showing sample collection locations and the areas excavated from 1937 to 2014.

### 3. Results and Discussion

#### 3.1. Mineralogical, Petrographic and Chemical Characterization

By observing the minero-petrographic features of the architectural earthenwares through microscopy (Tables 2 and 3) and XRPD (Table 4), a significant variability is visible among the samples. They are characterized by a light brown to reddish groundmass, which is generally optically isotropic and only in few cases optically active with a medium to low birefringent fabric (Table 2). In



samples S7, S13 and S18 the sandwich effect is also visible. The non-plastic inclusions show a size class [49] between fine sand (samples S10 and S17) and coarse sand (samples S3, S4 and S7) and a sorting [39,40] variable from moderately well sorted (samples S17 and S9) to poorly sorted (samples S3, S4 and S7). They are generally composed of under-saturated volcanic rocks' fragments (Figure 2a), where leucite and analcime crystals are clearly visible. The presence of analcime, inside the volcanic rocks' fragments, was also confirmed by Raman spectroscopy (Figure 3), and most probably, it is related to the alteration of the leucite crystals.

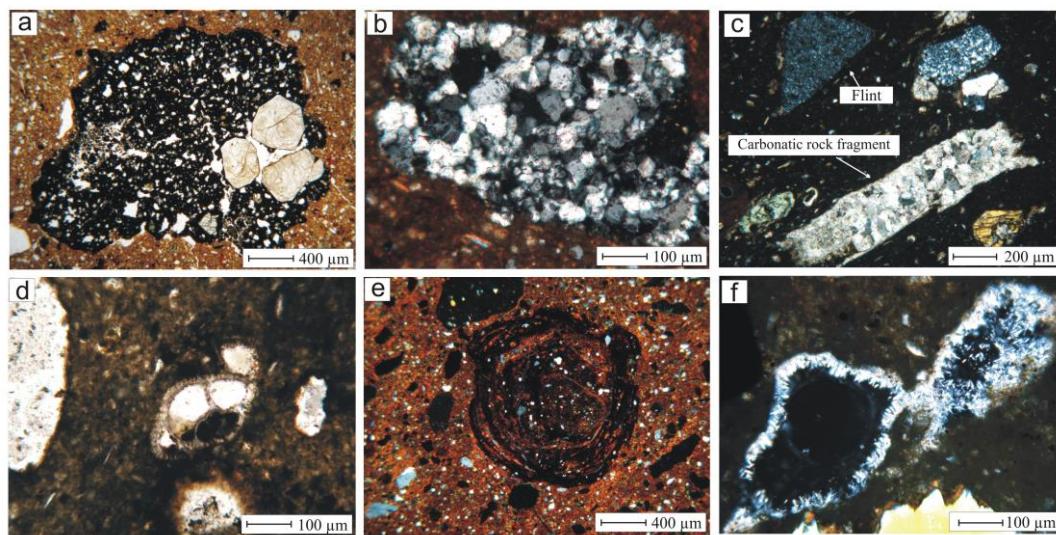


**Figure 2.** Microphotographs in thin section. All images are under crossed nicols, except for (a) and (d) which are under parallel nicols. (a) Volcanic rock fragment in sample S7. (b) Quartzite in sample S21. (c) Flint and carbonatic rock fragment in sample S12. (d) Bioclast in sample S13. (e) Argillaceous rock fragment (ARFs) in samples S3. (f) Secondary calcite inside porosity in sample S11.

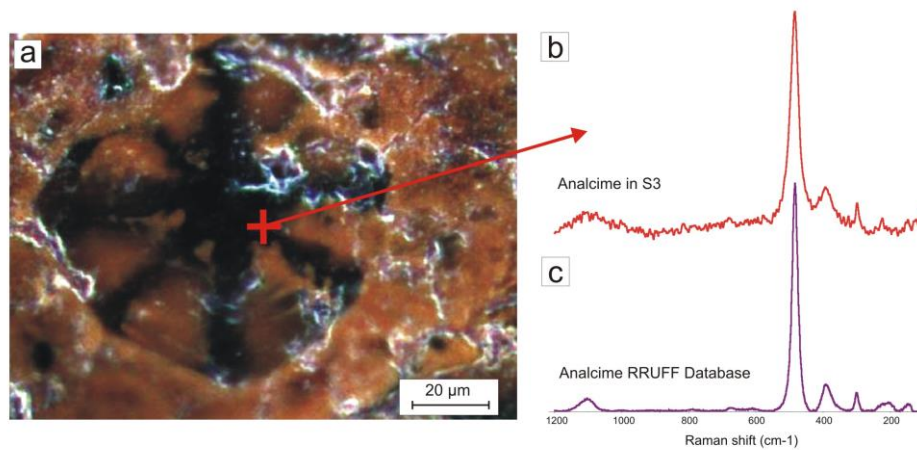


**Figure 3.** (a) OM image under reflected light of a dendritic-skeletal crystal of analcime inside a volcanic rock fragment in sample S3, showing the area analyzed by Raman spectroscopy. (b) Raman spectrum of the area analyzed. (c) Raman spectrum of the analcime from the RRUFF project database.

In addition to the under-saturated volcanic rocks' fragments, principally visible in samples S3, S4 and S7 (Figure 2a), quartzites (Figure 2b), phyllites, flints (Figure 2c), carbonatic rock fragments are also present in sample S12 (Figure 2c), traces of bioclasts (in particular Foraminifera) are present in samples S12, S13 (Figure 2d), S17, and S18 and argillaceous rock fragments (ARFs) [50] were found in samples S3 (Figure 2e), S4, and S7.

**Table 2.** Petrographic features of the architectural earthenwares by optical microscopy. (Roundness = HS: high sphericity, LS: low sphericity, A: angular, SA: sub-angular, SR: sub-rounded. Sorting = MS: moderately sorted, MWS: moderately well sorted, PS: poorly sorted, WS: well sorted. Optical aspect of the matrix = OA: optically active; OI: optically inactive.

By Polarized Microscopy										
Fabric	Sample	Mean Non-Plastic Inclusions Size ( $\mu\text{m}$ )	Max. Non-Plastic Inclusions Size ( $\mu\text{m}$ )	Mean Macro Porosity ( $\mu\text{m}$ )	Max. Macro Porosity ( $\mu\text{m}$ )	Size Class	Roundness of Non-Plastic Inclusions	Sorting of Non Plastic-Inclusions	Matrix Colour	Optical Aspect of the Matrix
Fab. 1	S3	844	3252	140	380	Coarse Sand	HS-SR	PS	Reddish	OA
	S4	667	2408	127	271	Coarse Sand	HS-SA	PS	Reddish	OA
	S7	865	3876	142	275	Coarse Sand	HS-SA	PS	Reddish	OA (sandwich effect)
Fab. 2	S21	340	1582	76	256	Medium Sand	HS-A	MS	Brownish	OA
	S22	319	1592	59	255	Medium Sand	LS-SR/HS-A	MS	Brownish	OA
	S23	344	1048	66	190	Medium Sand	LS-SA	MS	Brownish	OA
Fab. 3	S13	338	2086	51	130	Medium Sand	LS-SR/HS-SA	MS	Brown-reddish	OA (sandwich effect)
	S18	539	2230	106	373	Coarse Sand	LS-SA	MS	Brown-reddish	OA (sandwich effect)
Fab. 4	S15	590	2660	80	210	Coarse Sand	HS-A	MS	Brown-reddish	OI
Fab. 5	S9	268	1074	88	183	Medium Sand	HS-SA	MWS	Light brown	OI
Fab. 6	S10	238	1165	53	92	Fine Sand	HS/LS-SR	WS	Brownish	OI
Fab. 7	S11	321	2822	180	304	Medium Sand	HS/LS-SA	MS	Brownish	OI
Fab. 8	S12	423	2686	150	215	Medium Sand	HS-A	MS	Light brown	OI
Fab. 9	S17	166	1882	88	375	Fine Sand	HS-SA	MWS	Brownish	OA

**Table 3.** Mineralogical and petrographic features of the architectural earthenwares by optical microscopy and Semiquantitative visual estimation of non-plastic inclusions, matrix and macroporosity. Mineralogical phases = Anl: analcime, Bt: biotite, Cal: calcite, Cpx: clinopyroxene, Gh: gehlenite, Grt: garnet, Hem: hematite, Ill: illite, Kln: kaolinite, Lct: leucite, Ms: muscovite, Om: opaque minerals, Or: orthoclase, Pl: plagioclase, Qtz: quartz. tr: traces.

Fabric	Sample	Semiquantitative Visual Estimation by Polarized Microscopy				By Polarized Microscopy and XRPD		
		% Non-Plastic Inclusions (size > 1/16 mm)	% Matrix (size < 1/16 mm)	Matrix/Non-Plastic Inclusions Ratio	% Macro Porosity (size > 1/16 mm)	Mineralogical Phases of the Non-Plastic Inclusions	Rock Fragments	Other
Fab. 1	S3	15	75	5.0	10	Qtz, Cpx, Pl, Or, Anl, Ms, Bt, Om, Ill, Grt(tr)	Volcanic rocks, flints (tr)	ARFs
	S4	15	75	5.0	10	Qtz, Pl, Or, Cpx, Ms, Bt, Om, Grt(tr), Kln(tr)	Volcanic rocks	ARFs
	S7	20	65	3.3	15	Qtz, Pl, Or, Cpx, Anl, Bt, Om, Ill(tr), Grt(tr), Cal(tr)	Volcanic rocks	ARFs, secondary calcite inside porosity
Fab. 2	S21	20	65	3.3	15	Qtz, Cpx, Cal, Pl, Or, Ms, Bt, Anl, Om(tr), Grt(tr), Lct(tr)	Quartzites, volcanic rocks (tr)	Secondary calcite inside porosity
	S22	15	70	4.7	15	Qtz, Cal, Cpx, Pl, Lct, Ill, Bt, Om, Anl(tr), Grt(tr), Or(tr)	Quartzites, volcanic rocks (tr)	Secondary calcite inside porosity
	S23	20	65	3.3	15	Qtz, Cal, Cpx, Pl, Hem, Lct, Bt(tr), Grt(tr), Anl(tr)	Volcanic rocks (tr)	Secondary calcite inside porosity
Fab. 3	S13	25	62	2.5	13	Qtz, Cal, Pl, Cpx, Lct, Or, Gh, Om, Bt, Grt(tr), Anl(tr)	Volcanic rocks, flints	Secondary calcite inside porosity, bioclasts (tr)
	S18	18	69	3.8	13	Qtz, Cal, Cpx, Pl, Anl, Hem, Bt(tr), Grt(tr), Or (tr)	Volcanic rocks, flints	Secondary calcite inside porosity, bioclasts (tr)
Fab. 4	S15	20	65	3.3	15	Qtz, Cpx, Cal, Gh, Pl, Or, Hem, Lct, Bt(tr), Grt(tr)	Volcanic rocks, flints (tr), quartzites (tr)	Secondary calcite inside porosity
Fab. 5	S9	20	67	3.4	13	Qtz, Cpx, Pl, Cal, Or, Anl, Om, Bt, Grt(tr), Gh(tr), Hem(tr)	Volcanic rocks, quartzites	Secondary calcite inside porosity
Fab. 6	S10	40	40	1.0	20	Qtz, Cpx, Pl, Cal, Gh, Hem, Om, Ill, Grt, Bt(tr), Anl(tr)	Flints, quartzites, volcanic rocks, phyllites (tr)	Secondary calcite inside porosity
Fab. 7	S11	30	52	1.7	18	Qtz, Cpx, Cal, Gh, Pl, Or, Hem, Anl, Bt, Grt(tr)	Volcanic rocks, quartzites	Secondary calcite inside porosity
Fab. 8	S12	35	47	1.3	18	Qtz, Cal, Pl, Cpx, Or, Om, Ill(tr), Anl(tr), Bt(tr)	Flints, volcanic rocks, quartzites, carbonatic rocks	Secondary calcite inside porosity, bioclasts (tr)
Fab. 9	S17	30	50	1.7	20	Qtz, Cal, Pl, Cpx, Or, Om, Ms, Bt, Grt(tr)	Quartzites, filnts, volcanic rocks	Secondary calcite inside porosity, bioclasts (tr)

**Table 4.** Quantitative mineralogical composition of the architectural earthenwares by XRPD analysis and Rietveld refinements. nd: not detected.

wt. %	Quartz	Orthoclase	Clinopyroxene	Analcime	Leucite	Kaolinite	Calcite	Hematite	Gehlenite	Mica	Plagioclase	Total
S3	29.09	14.28	9.87	5.25	nd	nd	nd	nd	nd	26.83	14.69	100
S4	32.07	18.45	11.45	nd	nd	5.4	nd	nd	nd	8.79	23.84	100
S7	17.35	8.43	29.48	4.22	nd	nd	5.76	nd	nd	5.66	29.09	100
S9	18.93	nd	40.77	5.08	nd	nd	7.35	0.69	1.56	1.25	24.37	100
S10	18.95	nd	40.82	5.07	nd	nd	7.36	0.69	1.57	1.26	24.28	100
S11	12.97	3.75	34.75	3.45	nd	nd	10.77	0.52	9.91	1.27	22.59	100
S12	24.46	nd	25.85	7.04	nd	nd	18.52	nd	nd	3.88	20.24	100
S13	20.08	18.46	17.72	0.06	4.15	nd	23.26	nd	0.49	4.34	11.43	100
S15	19.37	10.85	23.92	nd	2.54	nd	10.81	1.29	5.48	1.65	24.1	100
S17	23.05	6.24	13.45	nd	nd	nd	9.45	nd	nd	12.15	35.66	100
S18	18.33	5.7	17.98	5.10	nd	nd	22.51	0.37	nd	5.76	24.26	100
S21	22.47	4.89	22.73	3.76	2.71	nd	10.34	nd	nd	6.27	26.83	100
S22	20.17	5.17	24.05	2.90	2.57	nd	15.89	nd	nd	9.05	20.22	100
S23	24.69	nd	16.98	0.77	2.75	nd	11.68	nd	nd	3.99	39.15	100



The main mineralogical phases are quartz, clinopyroxene, micas and plagioclases, which are present in all of the samples in varying amounts (Table 4), while orthoclase, leucite, analcime, kaolinite, calcite, garnet and hematite were only found in some samples (Tables 2 and 4). The presence of calcite is principally due to alteration phenomena; it is a secondary recrystallized calcite mostly precipitated inside the porosity (Figure 2f) during the burial and, only for samples S12, S13, S17, and S18, it is also linked to the presence of carbonatic rock fragments or bioclasts among the non-plastic inclusions (Table 3).

From a technological point of view, the mineralogical composition of the samples can be useful to obtain information about their firing temperature. For example, the presence of gehlenite, detected by XRPD analysis in samples S9, S10, S11, S13, and S15, led to hypothesize a firing temperature ranging from 900 °C to 1050 °C [51,52]. However, the presence of gehlenite in association with small amounts of illite, suggests a firing temperature slightly lower than 1050 °C (about 900–1000 °C).

Kaolinite is present only in sample S4 (Table 4); considering that this clay mineral is generally thermally stable up to 450–500 °C (even if strongly dehydroxylated) and it collapses at 750–800 °C, it is likely that the sample reached a low firing temperature of less than 700 °C. Another probable interpretation explaining the presence of kaolinite regards an exposure to maximum temperature, which was too short for kaolinite to be destroyed [53–58].

The presence of calcite, for most samples, is not significant in order to estimate their firing temperature because it is principally present as a secondary mineral, except for samples S12, S13, S17 and S18 where calcite is linked to the presence of carbonatic rock fragments or bioclasts (Table 3). Only for these samples is it possible to estimate a firing temperature lower than 700 °C [52].

With respect to the chemical composition of the major elements (Table 5), some differences can be observed among the samples. Al<sub>2</sub>O<sub>3</sub>, SiO<sub>2</sub>, TiO<sub>2</sub>, MgO and CaO show significant variability, which allow distinguishing of samples S3, S4, and S7 from all the others. These samples contain the highest values of Al<sub>2</sub>O<sub>3</sub> (between 20.11 and 21.93 wt %), SiO<sub>2</sub> (between 54.10 and 57.65 wt %) and TiO<sub>2</sub> (between 1.11 and 1.26 wt %) and the lowest contents of CaO (between 2.66 and 3.62 wt %) and MgO (between 1.68 and 2.07 wt %). The higher or lower amount of these elements is linked to the mineralogical and petrographic composition of the samples, which contain a high percentage of volcanic rock fragments and ARFs. On observing the trace elements reported in Table 6, several similarities can also be found between samples S3, S4, and S7, which have the highest amounts of Zr, Y, Rb, Ba, and Co.

**Table 5.** Chemical composition of major elements of the architectural earthenwares by XRF analysis, expressed in wt. %. LOI: loss on ignition at 950 °C.

wt. %	SiO <sub>2</sub>	TiO <sub>2</sub>	Al <sub>2</sub> O <sub>3</sub>	Fe <sub>2</sub> O <sub>3</sub>	MnO	MgO	CaO	Na <sub>2</sub> O	K <sub>2</sub> O	P <sub>2</sub> O <sub>5</sub>	LOI
S3	55.00	1.11	20.11	9.52	0.15	1.98	3.62	1.50	2.72	0.24	4.05
S4	54.10	1.26	20.33	9.66	0.11	1.68	3.22	0.96	2.67	0.36	5.65
S7	57.65	1.19	21.92	9.72	0.15	2.07	2.66	1.33	2.27	0.13	0.91
S9	52.73	0.66	13.92	7.66	0.10	3.82	15.12	1.08	1.64	0.17	3.10
S10	53.42	0.71	11.35	8.63	0.13	4.15	15.25	1.09	1.54	0.16	3.57
S11	48.43	0.64	11.30	8.68	0.16	3.94	18.36	0.97	1.71	0.27	5.54
S12	47.59	0.63	12.39	7.54	0.20	4.02	15.04	0.84	1.98	0.28	9.49
S13	46.13	0.68	11.70	8.54	0.21	3.48	17.02	0.57	2.60	0.24	8.83
S15	49.28	0.65	11.86	8.24	0.18	3.24	16.77	1.21	2.12	0.29	6.16
S17	50.11	0.71	12.44	7.82	0.15	3.27	14.53	0.70	2.34	0.27	7.66
S18	45.72	0.74	11.71	9.60	0.18	3.63	16.91	0.56	2.40	0.27	8.28
S21	49.52	0.73	12.06	8.34	0.16	4.14	15.87	0.72	2.15	0.22	6.09
S22	49.20	0.71	11.69	8.20	0.17	4.15	16.71	0.65	2.07	0.20	6.25
S23	49.52	0.73	12.16	8.38	0.18	3.28	15.58	0.67	2.27	0.24	6.99

**Table 6.** Chemical composition of trace elements of the architectural earthenwares by XRF analysis, expressed in ppm.

ppm	Nb	Zr	Y	Sr	Rb	Ce	Ba	La	Ni	Cr	V	Co
S3	79	468	41	467	364	133	1377	31	68	140	174	25
S4	103	530	41	374	341	117	1370	<20	79	156	142	31
S7	49	406	54	329	315	229	1992	168	98	156	154	28
S9	34	58	35	501	155	262	564	104	87	149	144	22
S10	23	127	31	452	111	170	325	77	72	243	196	22
S11	30	105	29	614	124	180	297	53	56	174	162	17
S12	47	96	23	434	124	116	331	<20	41	174	124	11
S13	50	160	28	561	141	157	400	<20	39	149	162	19
S15	40	136	31	558	156	168	410	40	53	139	127	19
S17	44	161	29	422	118	143	382	27	54	251	157	23
S18	44	180	27	489	116	127	204	<20	44	153	195	19
S21	36	131	32	454	123	142	260	29	65	159	159	25
S22	31	114	29	449	117	158	235	54	65	160	160	21
S23	39	141	29	385	127	117	247	24	59	172	133	20

The chemical data of the major and trace elements were processed by principal component analyses (PCA), thus obtaining the graph in Figure 4, which also shows the different fabrics of the earthenwares, identified by combining the PCA analysis with the mineralo-petrographic features observed by optical microscopy (OM) and XRPD. When identifying fabrics, it is important to use various analytical methods rather than the geochemistry alone, as chemically similar samples may show deceiving overlaps when, in fact, they differ from a petrographic point of view (e.g. fabrics 3, 8 and fabrics 2, 4, 9, in Figure 4). For this reason, the petrographic analysis by polarized optical microscopy proves to be a valuable tool for measuring compositional and textural differences. The petrographic features of the fabrics identified are listed below:

1st fabric: Includes samples S3, S4 and S7 (Figure 4), characterized by a reddish matrix optically active. The non-plastic inclusions are poorly sorted [39,40] with a coarse-sized sand [49] and a high sphericity [38,39]. Additionally, from a chemical point of view, these samples differ totally from the others, due to their high content of volcanic rock fragments (Figures 2a and 4) and ARFs (Figure 2e).

2nd fabric: Includes samples S21, S22, and S23 (Figure 4), characterized by a brownish matrix optically active. The non-plastic inclusions are moderately sorted [39,40], with a medium sand size [49] and they are principally composed of clinopyroxene crystals (Figure 4), traces of volcanic rock fragments and quartzites.

3rd fabric: Includes samples S13 and S18 (Figure 4), characterized by the sandwich effect. The non-plastic inclusions are moderately sorted [39,40] and composed of clinopyroxenes, volcanic rock fragments, flint, and traces of bioclasts (Figure 4).

4th fabric: includes only sample S15 characterized by a brown-reddish matrix optically inactive with non-plastic inclusions moderately sorted [39,40], angular and with a high sphericity [38,39]. By observing the graph in Figure 4, the sample (red circle) seems to be linked to the 2nd fabric (cluster which includes blue squares); however, sample S15 differs from the samples belonging to the 2nd fabric because of its greater percentage of volcanic rock fragments and the presence of flints (Figure 4).

5th fabric: Includes only sample S9 (Figure 4), which is characterized by a light brown matrix optically inactive. The non-plastic inclusions, moderately well sorted [39,40], have a medium sand size [49] and are sub-angular with high sphericity [38,39]. This sample is mainly composed of quartz and clinopyroxene crystals, volcanic rock fragments and quartzites.

6th fabric: Includes sample S10, which is the only sample characterized by an oriented porosity (Figure 4), created during pottery production. The sample is composed of a brownish matrix, optically inactive, which embeds well-sorted non-plastic inclusions [39,40], with a fine sand size [49]. The sample contains quartz and clinopyroxene crystals, flints, volcanic rocks' fragments, and traces of phyllites.

7th fabric: Includes only sample S11 (Figure 4), which is characterized by an optically inactive brownish matrix. The non-plastic inclusions have a medium sand size [49] and are moderately

sorted [39,40]. This sample contains the highest percentage of clinopyroxene crystals (Figure 4 and Table 4), as well as fragments of volcanic rocks and quartzites. Calcite recrystallization rims are sometimes present inside porosity (Figure 2f).

8th fabric: Is represented by sample S12, which has a light brown matrix optically inactive. The non-plastic inclusions have a medium sand size [49] and are moderately sorted [39,40], angular with high sphericity [38,39]. By observing the graph in Figure 4, the sample (black cross) seems to be linked to the 3rd fabric (purple rhombuses); however, it differs from it because it is characterized by the presence of rounded carbonate rock fragments, in addition to fragments of flint, quartzites, volcanic rocks, and bioclasts (Table 3 and Figure 4).

9th fabric: Includes sample S17. It is characterized by a brownish matrix optically active. The non-plastic inclusions have a fine sand size [49] and are moderately well sorted [39,40], sub angular, with high sphericity [38,39]. By observing the graph in Figure 4, the sample (blue hexagon) seems to match with the 2nd and the 4th fabrics (blue squares and red circle); however, this sample differs from the samples included in those fabrics because it is principally composed of quartz and plagioclases, which represent the main mineralogical associations (Figure 4 and Table 4), and it also contains fragments of quartzites, flints, volcanic rocks, and bioclasts (as traces).

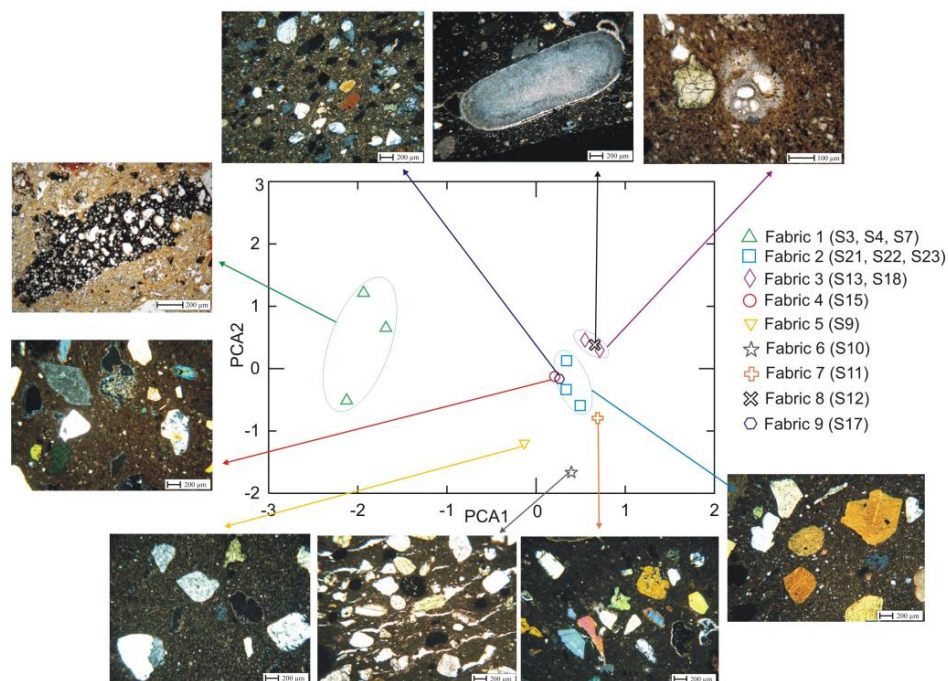


**Figure 4.** PCA component analysis, obtained by major and trace elements and microphotographs in thin section of the nine fabrics of the architectural earthenwares, identified by combining geochemical and petrographical data.

### 3.2. Provenance Hypothesis of the Raw Materials

The previous study performed by Ammerman et al. [37] already made hypotheses about the provenance of the clays used in some ceramic materials coming from the S. Omobono archaeological area. On the other hand, our work aims to provide information on the provenance of the degreasing used in the architectural earthenwares sampled.

The approach adopted, in this work, to formulate preliminary hypotheses about the provenance of the raw materials was to analyze the chemical composition of the primary clinopyroxenes. Firstly, the clinopyroxenes were identified by optical microscopy and Raman spectroscopy, and subsequently, they were studied with the electron probe micro analyzer (EPMA). In particular, three crystals of clinopyroxenes for each sample were analyzed by calculating the mean value of each one. The

classification of clinopyroxenes (Figure 5a) was carried out according to the International Mineralogical Association scheme [59], based on the content of enstatite ( $\text{MgSiO}_3$ ), ferrosilite ( $\text{FeSiO}_3$ ), and wollastonite ( $\text{CaSiO}_3$ ). As shown in Figure 5a, all the clinopyroxenes analyzed fall into the diopside field.

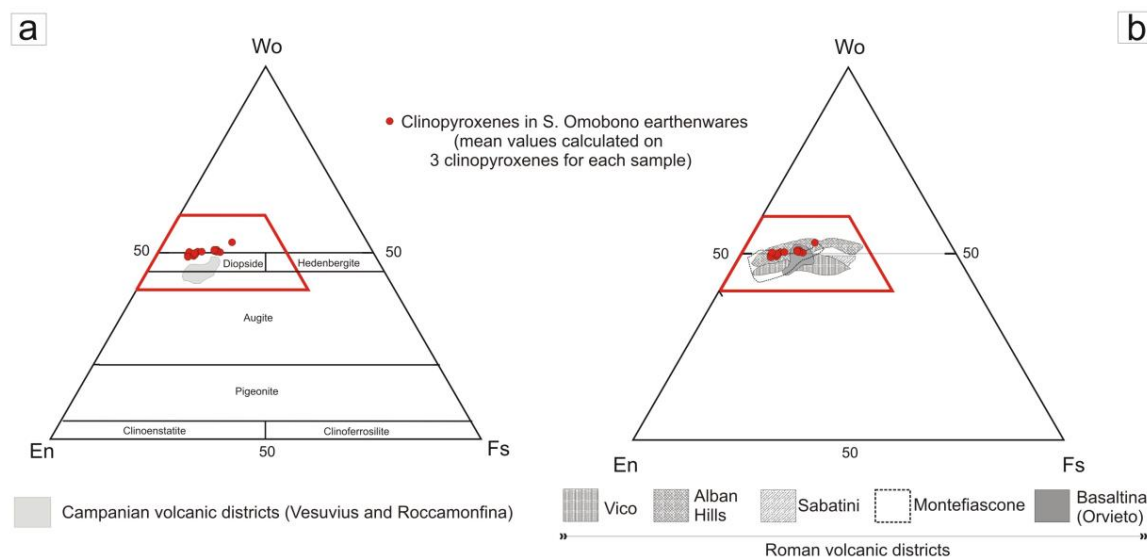


**Figure 5.** Classification of clinopyroxenes [59] using data obtained by EPMA and comparison between the composition of the clinopyroxenes analyzed in the archaeological samples of S. Omobono with those from the Campanian volcanic province (a) and the Roman volcanic complexes and districts (b).

In order to establish a local or alloctonous provenance of the raw materials, the chemical compositions of clinopyroxenes from Roman (Figure 5a) and Campanian (Figure 5b) volcanic provinces were taken into account using data present in literature [60–67]. By observing the diagrams in Figure 5b, it is likely that the clinopyroxenes compositions of the samples from S. Omobono overlap those of the clinopyroxenes belonging to the Roman volcanic province. Consequently, further comparisons were also made with several volcanic complexes and districts outcropping not far from Rome, using binary diagrams (Figure 6) with the variation of the major oxides [66]. Observing the CaO vs.  $\text{SiO}_2$  (Figure 6a) and CaO vs. FeO (Figure 6b) diagrams, a good affinity between the analyzed clinopyroxenes and those of the Bolsena Complex can be highlighted.

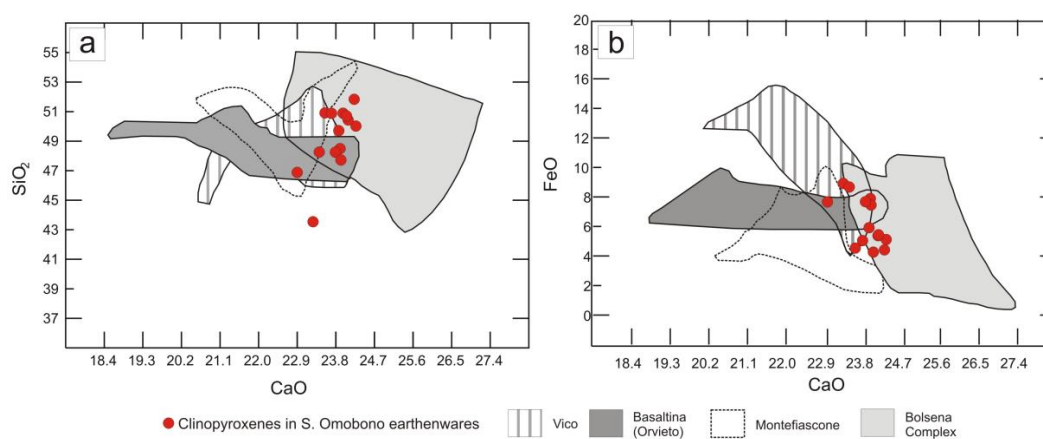


**Figure 6.** CaO vs.  $\text{SiO}_2$  (a) and CaO vs. FeO (b) diagrams showing the comparisons between the clinopyroxenes analyzed in the archaeological samples of S. Omobono and those found in some Roman volcanic districts [66].



However, the number of clinopyroxenes studied is too low to provide definitive results on their provenance; in fact, there are several literature data of Campanian pyroxenes that may overlap with Roman clinopyroxenes [68–71]. In the future, to have more detailed information on the origin of clinopyroxenes it could be useful to perform LA-ICP-MS analysis for determining their trace elements composition.

#### 4. Conclusions

Fourteen samples of architectural earthenwares coming from the archaeological area of S. Omobono were analyzed through a multi-analytical approach based on mineralogical, petrographic, chemical and statistical analyses. The combination of all the data collected enabled us to identify nine different fabrics, characterized by several typologies of non-plastic inclusions, which are present in the samples in different ratios with the matrix. The hypothesis of a local production of the architectural earthenware can be proposed. In particular, by comparing the clinopyroxenes compositions of the archaeological items with those of clinopyroxenes related to the Roman Magmatic Province [60–67], it appears that the non-plastic inclusion used in the earthenwares analyzed, probably came from the Bolsena Complex. However, these are only preliminary results and further in-depth studies are required on the clay quarries and the temper present in the surrounding area to clarify the exact provenance of the raw materials, as well as a chemical elaboration based on ancient mixing techniques of raw materials [9,16].

The great variability of the fabrics in the archaeological site led us to hypothesize that the raw materials came from four different quarries: the first quarry probably only contains volcanic rocks (fabric 1), the second quarry is mainly composed of clinopyroxenes (fabric 2), the third contains volcanic rocks and microfossils (fabrics 3, 9), while the fourth is composed of carbonatic rock fragments and bioclasts (fabric 8). For the other fabrics it is possible to hypothesize a raw material mixture resulting from natural geological processes or intentional human activity, obtained from the above-mentioned quarries. These results show that to understand the compositional variability of ceramic materials in an archaeological site, it is not sufficient to study only the archaeological materials, but an in depth study of all the probable quarries of clay and degreasings should be performed.

As regards the firing temperature of the samples, it is important to note that the materials found in the Roman Magmatic Province commonly contain diopside, therefore it is not possible to use it as a geo-thermometer. The presence of gehlenite, which was detected in samples S9, S10, S11, S13 and S15 allow us to hypothesize that these samples were fired at a temperature lower than 1050 °C (about 900–1000 °C) [51,52]. Sample S4, containing kaolinite, probably reached a low firing temperature of less than 700 °C or, it may have been exposed to a maximum temperature for a period of time that was too short to allow the destruction of the kaolinite [53–58]. Indeed, for samples S12, S13, S17, and S18, where primary calcite is present, it is possible to estimate a firing temperature lower than 700 °C [52].

From an archaeometric point of view the following conclusions can be drawn:

The fired roof tiles (impasto rosso pan-tile: samples S3, S4, S7; Table 1), belonging to the late Orientalizing phase (end of 7<sup>th</sup>-beginning of the 6<sup>th</sup> century BC), differ markedly from all of the later roof tiles. These data could be used in the future to extend the analysis to other archaeological sites and to investigate the compositional similarities or differences between the roof tiles (red-brown impasto pan-tile).

It is well known that in the Archaic phase (580–510 BC) red tile roofs (impasto rosso pan-tile) were replaced by roofs made with a light sand mixture (impasto chiaro sabbioso pan-tile). On observing the analytical data, we can see significant compositional variability in the impasto chiaro sabbioso pan-tiles; moreover, six different fabrics belong to this typology: fabric 3 (S13, S18), fabric 4 (S15), fabric 6 (S10), fabric 7 (S11), fabric 8 (S12), and fabric 9 (S17).

Fabric 2 (S21, S22, S23) includes architectural decorative elements, which, based on the archaeological analysis of scientific literature [72], have been divided into two distinct chronological phases: the first phase (580–560 BC), which includes samples S21 and S22, and the second one (540–530 BC), which includes sample S23. However, the compositional analyses show significant

compositional homogeneity, which is noteworthy because it suggests that further archaeological and archaeometric studies should be carried out on a larger cohort of samples. It is important to note how from a compositional point of view the three samples are clearly distinguished by the samples of pan-tile and cover-tile, thus indicating that there are differences between the roofs and their decorations, which is an aspect that requires further research in order to determine the cause.

The study showed that the archaeometric analyses of the architectural earthenwares not only contribute to define the evolution of these architectural manufacturing techniques, but also provide valuable insights on how to determine the construction phases of ancient buildings in the absence of joint mortars [73–77].

**Author Contributions:** P.B. and M.C. contributed in the archaeological part; D.M., F.A., A.B., S.C., R.D.L., M.L., A.P. and B.S.M. performed the analyses and analysed the data; D.M., P.B., M.C., F.A., A.B., S.C., R.D.L., M.L., A.P. and B.S.M. wrote the paper.

**Funding:** This research received no external funding.

**Acknowledgments:** Research on the archaeological site has been conducted since 2009 as part of an international collaboration between Sovrintendenza Capitolina, Department of Humanistic Studies of the University of Calabria and University of Michigan. The analyses were carried out in the Laboratories of the Department of Biology, Ecology and Earth Science (DiBEST) of the University of Calabria. The authors would like to thank Mariano Davoli and Giancarlo Niceforo for their valuable assistance as well as the Sovrintendenza Capitolina ai Beni Culturali di Roma Capitale.

**Conflicts of Interest:** The authors declare no conflict of interest.

## References

1. Pisani Sartorio, G.; Virgili, P.; Ioppolo, G. La scoperta dei Templi della Fortuna e della Mater Matuta. In *Il Viver Quotidiano in Roma Arcaica: Materiali dagli scavi del tempio arcaico nell'area sacra di S. Omobono*; Pisani Sartorio, G., Virgili, P., Ioppolo, G., Eds.; Edizioni Procom: Roma, Italy, 1989; pp. 13–15.
2. Mura, A.S. La decorazione architettonica del tempio arcaico. *La Parol. del Passato* **1977**, *32*, 62–71.
3. Colonna, G. Le due fasi del tempio arcaico di S. Omobono. In *Stips Votiva: Papers presented to C.M. Stibbe*; Gnade, M., Ed.; University of Amsterdam: Amsterdam, The Netherlands, 1991; pp. 51–59.
4. Brocato, P.; Ceci, M.; Terrenato, N. *Ricerche nell'area dei templi di Fortuna e Mater Matuta*; Dipartimento di Studi Umanistici dell'Università della Calabria: Rende, Italy, 2016.
5. Brocato, P.; Terrenato, N. *Nuove ricerche nell'area archeologica di S. Omobono*; Dipartimento di Studi Umanistici dell'Università della Calabria: Rende, Italy, 2012.
6. Terrenato, N.; Brocato, P.; Caruso, G.; Ramieri, A.M.; Becker, H.W.; Cangemi, I.; Mantiloni, G.; Regoli, C. The S. Omobono Sanctuary in Rome: Assessing eighty years of fieldwork and exploring perspectives for the future. *Internet Archaeol.* **2012**, *31*. [[CrossRef](#)]
7. Maggetti, M. *Mineralogical and Petrographical Methods for the Study of Ancient Pottery*; Università La Sapienza: Roma, Italy, 1994.
8. Belfiore, C.M.; Day, P.M.; Hein, A.; Kilikoglou, V.; La Rosa, V.; Mazzoleni, P.; Pezzino, A. Petrographic and chemical characterization of pottery production of the Late Minoan I kiln at Haghia Triada, Crete. *Archaeometry* **2007**, *49*, 621–653. [[CrossRef](#)]
9. Miriello, D.; Crisci, G.M. Mixing and provenance of raw materials in the bricks from the Svevian castle of Rocca Imperiale (North Calabria, Italy). *Eur. J. Mineral.* **2007**, *19*, 137–144. [[CrossRef](#)]
10. Lindsay, I.; Minc, L.; Descantes, C.; Speakman, R.J.; Glascock, M.D. Exchange patterns, boundary formation, and sociopolitical change in Late Bronze Age Southern Caucasia: Preliminary results from a pottery provenance study in northwestern Armenia. *J. Archaeol. Sci.* **2008**, *35*, 1673–1682. [[CrossRef](#)]
11. Barone, G.; Belfiore, C.M.; Mazzoleni, P.; Pezzino, A.; Viccaro, M. A volcanic inclusions based approach for provenance studies of archaeological ceramics: Application to pottery from southern Italy. *J. Archaeol. Sci.* **2010**, *37*, 713–726. [[CrossRef](#)]
12. Scarpelli, R.; De Francesco, A.M.; Perri, F.; Osanna, M.; Colangelo, L.; Miriello, D.; La Russa, M.F.; Barca, D.; Crisci, G.M. Archaeometric study of sub-geometric pottery found in Potenza, Italy: Relationship and trade between near indigenous centers. *Period. Mineral.* **2010**, *79*, 81–94.



13. Montana, G.; Cau Ontiveros, M.Á.; Polito, A.M.; Azzaro, E. Characterisation of clayey raw materials for ceramic manufacture in ancient Sicily. *Appl. Clay Sci.* **2011**, *53*, 476–488. [[CrossRef](#)]
14. Cau Ontiveros, M.Á.; Montana, G.; Tsantini, E.; Randazzo, L. Ceramic Ethnoarchaeometry in Western Sardinia: Production of Cooking Ware at Pabillonis. *Archaeometry* **2015**, *57*, 453–475. [[CrossRef](#)]
15. Cano, N.F.; Ribeiro, R.B.; Munita, C.S.; Watanabe, S.; Neves, E.G.; Tamanaha, E.K. Dating and determination of firing temperature of ancient potteries from São Paulo II archaeological site, Brazil by TL and EPR techniques. *J. Cult. Herit.* **2015**, *16*, 361–364. [[CrossRef](#)]
16. Miriello, D.; Bloise, A.; De Luca, R.; Apollaro, C.; Crisci, G.M.; Medaglia, S.; Grasso, A.T. First compositional evidences on the local production of Dressel 2–4 amphorae in Calabria (Southern Italy): Characterization and mixing simulations. *Appl. Phys. A Mater. Sci. Process.* **2015**, *119*, 1595–1608. [[CrossRef](#)]
17. Taranto, M.; Barba, L.; Blancas, J.; Bloise, A.; Cappa, M.; Chiaravalloti, F.; Crisci, G.M.; Cura, M.; De Angelis, D.; De Luca, R.; Lezzerini, M.; Pecci, A.; Miriello, D. The bricks of Hagia Sophia (Istanbul, Turkey): A new hypothesis to explain their compositional difference. *J. Cult. Herit.* **2019**. [[CrossRef](#)]
18. Columbu, S.; Sitzia, F.; Verdiani, G. Contribution of petrophysical analysis and 3D digital survey in the archaeometric investigations of the Emperor Hadrian's Baths (Tivoli, Italy). *Rend. Lincei* **2015**, *26*, 455–474. [[CrossRef](#)]
19. Columbu, S.; Sitzia, F.; Ennas, G. The ancient pozzolanic mortars and concretes of Heliocaminus baths in Hadrian's Villa (Tivoli, Italy). *Archaeol. Anthr. Sci.* **2017**, *9*, 523–553. [[CrossRef](#)]
20. Columbu, S.; Palomba, M.; Sitzia, F.; Murgia, M. Geochemical and mineral-petrographic studies of stones and mortars from the Romanesque Saccargia Basilica (Sardinia, Italy) to define their origin and alteration. *Ital. J. Geosci.* **2018**, *137*, 369–395. [[CrossRef](#)]
21. Ramacciotti, M.; Rubio, S.; Gallelo, G.; Lezzerini, M.; Columbu, S.; Hernandez, E.; Morales-Rubio, A.; Pastor, A.; De La Guardia, M. Chronological classification of ancient mortars employing spectroscopy and spectrometry techniques: Sagunto (Valencia, Spain) Case. *J. Spectrosc.* **2018**. [[CrossRef](#)]
22. Columbu, S.; Lisci, C.; Sitzia, F.; Lorenzetti, G.; Lezzerini, M.; Pagnotta, S.; Raneri, S.; Legnaioli, S.; Palleschi, V.; Gallelo, G.; et al. Mineralogical, petrographic and physical-mechanical study of Roman construction materials from the Maritime Theatre of Hadrian's Villa (Rome, Italy). *Measurement* **2018**, *127*, 264–276.
23. Columbu, S.; Garau, A.M.; Lugliè, C. Geochemical characterisation of pozzolanic obsidian glasses used in the ancient mortars of Nora Roman theatre (Sardinia, Italy): Provenance of raw materials and historical–archaeological implications. *Archaeol. Anthropol. Sci.* **2018**, 1–30. [[CrossRef](#)]
24. Columbu, S.; Garau, A.M. Mineralogical, petrographic and chemical analysis of geomaterials used in the mortars of Roman Nora theatre (south Sardinia, Italy). *Ital. J. Geosci.* **2017**, *136*, 238–262. [[CrossRef](#)]
25. Raneri, S.; Pagnotta, S.; Lezzerini, M.; Legnaioli, S.; Palleschi, V.; Columbu, S.; Neri, N.F.; Mazzoleni, P. Examining the reactivity of volcanic ash in ancient mortars by using a micro-chemical approach. *Mediterr. Archaeol. Archaeom.* **2018**, *18*, 147–157.
26. Columbu, S.; Gioncada, A.; Lezzerini, M.; Marchi, M. Hydric dilatation of ignimbritic stones used in the Church of Santa Maria di Otti (Oschiri, northern Sardinia, Italy). *Ital. J. Geosci.* **2014**, *133*, 149–160. [[CrossRef](#)]
27. Antonelli, F.; Columbu, S.; De Vos Raaijmakers, M.; Andreoli, M. An archaeometric contribution to the study of ancient millstones from the Mulargia area (Sardinia, Italy) through new analytical data on volcanic raw material and archaeological items from Hellenistic and Roman North Africa. *J. Archaeol. Sci.* **2014**, *50*, 243–261. [[CrossRef](#)]
28. Columbu, S.; Lisci, C.; Sitzia, F.; Buccellato, G. Physical-mechanical consolidation and protection of Miocenic limestone used on Mediterranean historical monuments: The case study of Pietra Cantone (southern Sardinia, Italy). *Environ. Earth Sci.* **2017**, *76*, 148. [[CrossRef](#)]
29. Verdiani, G.; Columbu, S. EStone, an Archive for the Sardinia Monumental Witnesses. *Lect. Notes Comput. Sci.* **2010**, *6436*, 356–372.
30. Columbu, S. Petrographic and geochemical investigations on the volcanic rocks used in the Punic-Roman archaeological site of Nora (Sardinia, Italy). *Environ. Earth Sci.* **2018**, *77*, 577. [[CrossRef](#)]
31. Antonelli, F.; Columbu, S.; Lezzerini, M.; Miriello, D. Petrographic characterization and provenance determination of the white marbles used in the Roman sculptures of Forum Sempronii (Fossombrone, Marche, Italy). *Appl. Phys. A Mater. Sci. Process.* **2014**, *115*, 1033–1040. [[CrossRef](#)]

32. Columbu, S. Provenance and alteration of pyroclastic rocks from the Romanesque Churches of Logudoro (north Sardinia, Italy) using a petrographic and geochemical statistical approach. *Appl. Phys. A Mater. Sci. Process.* **2017**, *123*, 1–28. [[CrossRef](#)]
33. Columbu, S.; Antonelli, F.; Sitzia, F. Origin of Roman worked stones from St. Saturno Christian Basilica (south Sardinia, Italy). *Mediterr. Archaeol. Archaeom.* **2018**, *18*, 17–36.
34. Columbu, S.; Piras, G.; Sitzia, F.; Pagnotta, S.; Raneri, S.; Legnaioli, S.; Palleschi, V.; Lezzerini, M.; Giamello, M. Petrographic and mineralogical characterization of volcanic rocks and surface-depositions on Romanesque monuments. *Mediterr. Archaeol. Archaeom.* **2018**, *18*, 37–63.
35. Coarelli, F. *Il Foro Boario: Dalle origini alla fine della Repubblica*; Quasa: Roma, Italy, 1988.
36. Brocato, P.; Diffendale, D.; Di Giuliomaria, D.; Gaeta, M.; Marra, F.; Terrenato, N. Identification of a previously unknown tuff for the construction of the archaic Temple Podium at Sant’Omobono, Rome. *J. Mediterr. Archaeol.* **2019**, in press.
37. Ammerman, A.J.; Iliopoulos, I.; Bondioli, F.; Filippi, D.; Hilditch, J.; Manfredini, A.; Pennisi, L.; Winter, N. The clay beds in the Velabrum and the earliest tiles in Rome. *J. Rom. Archaeol.* **2008**, *21*, 7–30. [[CrossRef](#)]
38. Powers, M.C. A new roundness scale for sedimentary particles. *J. Sediment. Res.* **1953**, *23*, 117–119. [[CrossRef](#)]
39. Boggs, S. *Petrology of Sedimentary Rocks*; Cambridge University Press: Cambridge, UK, 2010.
40. Jerram, D.A. Visual comparators for degree of grain-size sorting in two and three-dimensions. *Comput. Geosci.* **2001**, *27*, 485–492. [[CrossRef](#)]
41. Ricci Lucchi, F. *Sedimentologia Parte I: Materiali e Tessiture dei Sedimenti*; Cooperativa Libreria Universitaria: Bologna, Italy, 1980.
42. Best, M.G. *Igneous and Metamorphic Petrology*, 2nd ed.; Blackwell Publishing: Hoboken, NJ, USA, 2013.
43. Bloise, A.; Abd El Salam, S.; De Luca, R.; Crisci, G.M.; Miriello, D. Flux growth and characterization of cuprorivaite: The influence of temperature, flux and silica source. *Appl. Phys. A Mater. Sci. Process.* **2016**, *122*, 1–8. [[CrossRef](#)]
44. Rietveld, H. A profile refinement method for nuclear and magnetic structures. *J. Appl. Cryst.* **1969**, *2*, 65–71. [[CrossRef](#)]
45. Young, R.A. Introduction to the Rietveld method. In *The Rietveld Method*; Young, R.A., Ed.; Oxford University Press: Oxford, UK, 1993; pp. 1–38.
46. Aitchison, J. The statistical analysis of compositional data (with discussion). *J. R. Stat. Soc. Series B Stat. Methodol.* **1982**, *44*, 139–177.
47. Aitchison, J. The Principal component analysis of compositional data. *Biometrika* **1983**, *70*, 57–65. [[CrossRef](#)]
48. Aitchison, J. *The Statistical Analysis of Compositional Data*; Monographs on Statistics and Applied Probability; Chapman & Hall Ltd, London Reprinted (2003) with Additional Material by The Blackburn Press: Caldwell, NJ, USA, 1986.
49. Wentworth, C.K. A scale of grade and class terms for clastic sediments. *J. Geol.* **1922**, *30*, 377–392. [[CrossRef](#)]
50. Whitbread, I.K. The characterisation of argillaceous inclusions in ceramic thin sections. *Archaeometry* **1986**, *28*, 79–88. [[CrossRef](#)]
51. Peters, T.J.E.R.K.; Iberg, R. Mineralogical changes during firing of calcium-rich brick clays. *Ceram. Bull.* **1978**, *57*, 503–509.
52. Riccardi, M.P.; Messiga, B.; Duminuco, P. An approach to the dynamics of clay firing. *Appl. Clay Sci.* **1999**, *15*, 393–409. [[CrossRef](#)]
53. Dondi, M.; Ercolani, G.; Guarini, G.; Marsigli, M.; Venturi, I. Evoluzione della microstruttura durante la cottura rapida di impasti per piastrelle porose. *Ceramurgia* **1995**, *25*, 301–314.
54. Rice, P.M. *Pottery Analysis: A Sourcebook*; University of Chicago Press: Chicago, IL, USA, 2015.
55. De Bonis, A.; Cultrone, G.; Grifa, C.; Langella, A.; Morra, V. Clays from the Bay of Naples (Italy): New insight on ancient and traditional ceramics. *J. Eur. Ceram. Soc.* **2014**, *34*, 3229–3244. [[CrossRef](#)]
56. Grifa, C.; Germinario, C.; De Bonis, A.; Mercurio, M.; Izzo, F.; Pepe, F.; Bareschino, P.; Cucciniello, C.; Monetti, V.; Morra, V.; et al. Traditional brick productions in Madagascar: From raw material processing to firing technology. *Appl. Clay Sci.* **2017**, *150*, 252–266. [[CrossRef](#)]
57. Maggetti, M.; Neururer, C.; Ramseyer, D. Temperature evolution inside a pot during experimental surface (bonfire) firing. *Appl. Clay Sci.* **2011**, *53*, 500–508. [[CrossRef](#)]
58. De Bonis, A.; D’Angelo, M.; Guarino, V.; Massa, S.; Anaraki, F.S.; Genito, B.; Morra, V. Unglazed pottery from the masjed-i jom’ e of Isfahan (Iran): Technology and provenance. *Archaeol. Anthr. Sci.* **2017**, *9*, 617–635. [[CrossRef](#)]

59. Peccerillo, A.; Perugini, D. *Introduzione Alla Petrografia Ottica*; Morlacchi Editore: Perugia, Italy, 2003.
60. Negro, A.D.; Carbonin, S.; Salviulo, G.; Piccirillo, E.M.; Cundari, A. Crystal Chemistry and Site Configuration of the Clinopyroxene from Leucite-bearing Rocks and Related Genetic Significance: The Sabatini Lavas, Roman Region, Italy. *J. Petrol.* **1985**, *26*, 1027–1040. [[CrossRef](#)]
61. Aurisicchio, C.; Federico, M.; Gianfagna, A. Clinopyroxene chemistry of the high-potassium suite from the Alban Hills, Italy. *Mineral. Petrol.* **1988**, *39*, 1–19.
62. Querci, D. Studio di alcuni litotipi messi in opera nel Duomo di Orvieto (Terni): Caratteristiche chimico-fisiche e confronto con i materiali prelevati in cava. Ph.D. Thesis, University of Perugia, Perugia, Italy, 1995.
63. Di Battistini, G.; Montanini, A.; Bargossi, G.M.; Vernia, L.; Castorina, F. Petrology and geochemistry of ultrapotassic rocks from the Montefiascone Volcanic Complex (Central Italy): Magmatic evolution and petrogenesis. *Lithos* **1998**, *43*, 169–195. [[CrossRef](#)]
64. Perini, G.; Conticelli, S.; Francalanci, L.; Davidson, J.P. The relationship between potassic and calc-alkaline post-orogenic magmatism at Vico volcano, central Italy. *J. Volcanol. Geotherm. Res.* **2000**, *95*, 247–272. [[CrossRef](#)]
65. Scarpelli, R.; De Francesco, A.M.; Gaeta, M.; Cottica, D.; Toniolo, L. The provenance of the Pompeii cooking wares: Insights from LA-ICP-MS trace element analyses. *Microchem. J.* **2015**, *119*, 93–110. [[CrossRef](#)]
66. Comodi, P.; Nazzareni, S.; Perugini, D.; Bergamini, M. Technology and Provenance of roman ceramics from Scoppieto, Italy: A mineralogical and petrological study. *Period. Mineral.* **2006**, *75*, 95–112.
67. Nappi, G.; Antonelli, F.; Coltorti, M.; Milani, L.; Renzulli, A.; Siena, F. Volcanological and petrological evolution of the Eastern Vulcini District, Central Italy. *J. Volcanol. Geotherm. Res.* **1998**, *87*, 211–232. [[CrossRef](#)]
68. Antonelli, F.; Nappi, G.; Lazzarini, L. Roman millstones from Orvieto (Italy): Petrographic and geochemical data for a new archaeometric contribution. *Archaeometry* **2001**, *43*, 167–189. [[CrossRef](#)]
69. Santi, P.; Antonelli, F.; Renzulli, A.; Pensabene, P. Leucite phonolite millstones from the Orvieto production centre: New data and insights into the Roman trade. *Period. Mineral.* **2003**, *73*, 57–69.
70. Antonelli, F.; Lazzarini, L. Mediterranean trade of the most widespread Roman volcanic millstones from Italy and petrochemical markers of their raw materials. *J. Archaeol. Sci.* **2010**, *37*, 2081–2092. [[CrossRef](#)]
71. Morra, V.; Calcaterra, D.; Cappelletti, P.; Colella, A.; Fedele, L.; De’Gennaro, R.; Langella, A.; Mercurio, M. Urban geology: Relationships between geological setting and architectural heritage of the Neapolitan area. *J. Virtual Explor.* **2010**, *36*. [[CrossRef](#)]
72. Cristofani, M. Osservazioni sulle decorazioni fittili arcaiche dal santuario di Sant’Omobono. *Archeol. Laz.* **1989**, *10*, 31–37.
73. Barca, D.; Miriello, D.; Pecci, A.; Barba, L.; Ortiz, A.; Manzanilla, L.R.; Blancas, J.; Crisci, G.M. Provenance of glass shards in archaeological lime plasters by LA-ICP-MS: Implications for the ancient routes from the Gulf of Mexico to Teotihuacan in Central Mexico. *J. Archaeol. Sci.* **2013**, *40*, 3999–4008. [[CrossRef](#)]
74. De Luca, R.; Gigliotti, V.; Panarello, M.; Bloise, A.; Crisci, G.M.; Miriello, D. Spectroscopic, microchemical and petrographic analyses of plasters from ancient buildings in Lamezia Terme (Calabria, Southern Italy). *Spectrochim. Acta Part A.* **2016**, *153*, 184–193. [[CrossRef](#)]
75. Miriello, D.; Barba, L.; Blancas, J.; Bloise, A.; Cappa, M.; Cura, M.; De Angelis, D.; De Luca, R.; Pecci, A.; Taranto, M.; et al. New compositional data on ancient mortars from Hagia Sophia (Istanbul, Turkey). *Archaeol. Anthropol. Sci.* **2017**, *9*, 499–514. [[CrossRef](#)]
76. Miriello, D.; De Luca, R.; Bloise, A.; Dattola, L.; Mantella, G.; Gazineo, F.; De Natale, A.; Iannelli, M.T.; Cuteri, F.A.; Crisci, G.M. Compositional study of mortars and pigments from the “Mosaico della Sala dei Draghi e dei Delfini” in the archaeological site of Kaulonía (Southern Calabria, Magna Graecia, Italy). *Archaeol. Anthropol. Sci.* **2017**, *9*, 317–336. [[CrossRef](#)]
77. Miriello, D.; Bloise, A.; Crisci, G.M.; De Luca, R.; De Nigris, B.; Martellone, A.; Osanna, M.; Pace, R.; Pecci, A.; Ruggieri, N. New compositional data on ancient mortars and plasters from Pompeii (Campania – Southern Italy): Archaeometric results and considerations about their time evolution. *Mater. Charact.* **2018**, *146*, 189–203. [[CrossRef](#)]

